A multi-fidelity framework for the estimation of the turbulent Schmidt number in the simulation of atmospheric dispersion

Riccardo Longo*[a,b], Aurélie Bellemans[a,c,d], Marco Derudi[b], Alessandro Parente[a,c]

[a] *Université libre de Bruxelles - Ecole Polytechnique de Bruxelles - Département d'Aéro-Thermo-Mécanique*
[b] *Politecnico di Milano - Dipartimento di Chimica, Materiali ed Ingegneria Chimica "G. Natta"*
[c] *Combustion and Robust Optimization Group (BURN), Université libre de Bruxelles and Vrjie Universiteit Brussel*
[d] *University of Texas at Austin - Department of Aerospace Engineering and Engineering Mechanics*

Abstract

A multi-fidelity framework is presented to accurately predict the turbulent Schmidt number, Sc_t with applications to atmospheric dispersion modelling. According to the literature and experimental evidence, different physical correlations can be traced for Sc_t, relating this quantity to various turbulent parameters. The objective is to derive a reliable formulation for Sc_t that can be used in various test cases and combined with several turbulence models in the context of Reynolds-averaged Navier-Stokes (RANS) simulations. To achieve that, high-fidelity data are obtained with a delayed Detached Eddy Simulation (dDES) and used in a correlation study to analyze the inter-dependencies of Sc_t with important turbulent variables. A first data-driven model for Sc_t is proposed by calibrating the data to the semi-empirical relation by Reynolds. A second model is presented using the results of a correlation study in combination with Principal Component Analysis (PCA). Both data-driven models were verified with the RANS simulation of the Cedval A1-5 case, and 2 additional dispersion cases: the Cedval B1-1 array of building, and the empty street canyon from the CODASC database. There can be concluded that the resulting Sc_t formulation is able to significantly improve the accuracy of the concentration field compared to standard RANS approaches. Furthermore, the validity of the new formulation is demonstrated in combination with several turbulence models.

Keywords

Urban Environment; Atmospheric Boundary Layer; Turbulent Schmidt Number; Multi-fidelity framework; Data-driven; Principal Component Analysis

*Corresponding author's email: riccardo.longo@ulb.ac.be ; alessandro.parente@ulb.be

Nomenclature

Symbol	Description
a, b, c, d, e, f	coefficients in Sc_t formulations
$\mathbf{A}, \mathbf{B}$	matrix of eigenvectors
$\bar{C}$	mean substance concentration, ppm
C_0, C	positive diffusion parameters
C_{k1}, C_{k2}	constant in the k inlet profile
C_1, C_2, m, n	constants in Sc_t formulation by Reynolds
C_k	substance concentration, ppm
C_m	measured tracer concentration, ppm
C_s	source tracer concentration, ppm
$C_\mu, C_{\epsilon 1}, C_{\epsilon 2}, \sigma_\epsilon$	constants in the $k-\epsilon$ model
D, H, W, L	building's dimensions, m
D_m	molecular diffusivity, $m^2 s^{-1}$
D_t	turbulent diffusivity, $m^2 s^{-1}$
F_S	safety factor
k	turbulent kinetic energy, $m^2 s^{-2}$
K	dimensionless concentration
$\mathbf{L}$	vector of eigenvalues
n	number of observations
Pe	Péclet number
Pr	Prandtl number
Q	number of conserved variables
Q_l	emission rate of line source, $m^2 s^{-1}$
Q_s	total source flow rate, $m^3 s^{-1}$
r_h	coarsening ratio
Re	Reynolds number
Re_λ	Reynolds at the Taylor micro-scale
Re_t	turbulent Reynolds number
S	strain-rate invariant

Sc	molecular Schmidt number
Sc_t	turbulent Schmidt number
u_x, u_y, u_z	velocity components, $m\ s^{-1}$
u_*	ABL friction velocity, $m\ s^{-1}$
x, y, z	stream-wise, width and height coordinates, m
x_i	measured tracer molar fraction
$\mathbf{X}$	matrix of samples
$\widetilde{y}^+, y^+$	non-dimensional wall distances
z_0	aerodynamic roughness length, m
$\delta_u, \delta_k, \delta_h$	local deviation of turbulent properties
ϵ	turbulent dissipation rate, $m^2 s^{-3}$
κ	von Karman constant
μ_t	dynamic turbulent viscosity, $kg\ m^{-1} s^{-1}$
ν	kinematic molecular viscosity, $m^2 s^{-1}$
ν_t	kinematic turbulent viscosity, $m^2 s^{-1}$
ω	specific rate of turbulence dissipation, s^{-1}
Ω	vorticity invariant
ρ	density, $kg\ m^{-3}$

1. Introduction

The study of atmospheric dispersion is of major relevance to assess the air quality in urban environments. The major sources to urban air pollution are traffic (25%), combustion and agriculture (22%), domestic fuel burning (20%), natural dust (18%) and industrial activities (15%) [1]. Atmospheric dispersion models can be employed to determine the consequences of accidental chemical releases [2, 3, 4, 5, 6, 7]. Computational fluid dynamics (CFD) has been acknowledged as a powerful tool to predict urban flows [8] and dispersion patterns [9, 10, 11, 12, 13]. CFD dispersion modelling requires the definition of Sc_t, expressing the ratio of turbulent viscosity to mass diffusivity. However, the literature does not report clear guidelines on the definition of this parameter [14, 15, 16, 17]. Nevertheless, the importance of Sc_t was largely demonstrated [18, 19, 20, 21]. For Atmospheric Boundary Layer (ABL) flows, typical values range between 0.2 and 1.3 [22]. Reynolds [23] proposed an empirical formulation for the definition of Sc_t in function of the molecular Sc and the eddy viscosity ratio. The local variability of Sc_t is supported by experimental evidence [24, 25], suggesting that Sc_t should be prescribed as a dynamic variable [26, 27, 28]. In this regard, Gorlé et al. [29] developed a local Sc_t. The latter depends on C_μ and on the Reynolds number at the Taylor micro-scale. Subsequently, Longo et al. [15] proposed a Sc_t formulation depending on C_μ whose main dispersion parameters were optimized through uncertainty quantification. Di Bernardino et al. [25] found a reasonable agreement between their Sc_t measurements and the outcomes of the Sc_t formulation by Longo et al. [15]. The experimental observations [25] and the latest variable Sc_t formulations [29, 15] open the way to the present research.

A multi-fidelity framework combines computationally expensive high-fidelity simulations with simplified lower-order approximations to achieve affordable predictions at a desired user-defined accuracy [30, 31]. In the present framework, high-fidelity data are obtained using delayed Detached Eddy Simulations (dDES) and processed to develop a reliable model for Sc_t. The data-driven formulation for Sc_t is used afterwards in Reynolds-Averaged Navier-Stokes (RANS) simulations, characterized by a lower fidelity. Two strategies are investigated to develop a data-driven model for Sc_t. The first method calibrates the high-fidelity data to a prescribed model form, following the semi-empirical formulation by Reynolds [23]. The second strategy relies on Principal Component Analysis (PCA) to optimally correlate Sc_t to a significant number of model parameters.

PCA is a processing technique that allows to extract the main features in large multivariate data structures. The method can be used to derive a smaller set of correlated variables containing most of the variance of

the system. This subset of components can be used to retrieve and interpret important flow features or build reduced-order models [32, 33, 34]. Coussement et al. [35] proposed a technique, the Manifold Generated PCA (MG-PCA) method, where a subset of the original state-space variables is retained. The correlations between all variables is retrieved by using the information contained in the PCA matrices. In the present investigation, MG-PCA is used to optimally correlate a subset of relevant turbulent quantities involved in the dispersion phenomenon with Sc_t. It will be demonstrated how the MG-PCA based Sc_t formulation is able to improve the accuracy of dispersion prediction compared to standard approaches.

The novelty of this paper resides in the use of a comprehensive data-driven approach starting from high-fidelity data obtained with a dDES to derive a generalized Sc_t formulation. The latter can be successfully employed in conjunction with different RANS methodologies without limiting its local variability.

The paper is structured as follows: Section 2 details the turbulence and dispersion modelling of the ABL and presents the simulation test cases (Figure 1): (1) Cedval A1-5, a single building, (2) B1-1, an array of buildings [36], and (3) an empty street canyon from the CODASC database [37]. Section 3 explains the basics of principal component analysis. The results of the present data-driven approach in a multi-fidelity framework are presented in Section 4. The results section starts with the calibration of the high-fidelity data to the semi-empirical formula of Reynolds [23]. Next, an optimized formulation for Sc_t is derived after a correlation analysis and the use of MG-PCA. Finally, the resulting Sc_t formulations are validated on different cases in combination with various turbulence formulations. The novel approach demonstrates superior performance albeit its coupling to turbulence models that are not optimized for ABL flows. Conclusions are drawn in Section 5.

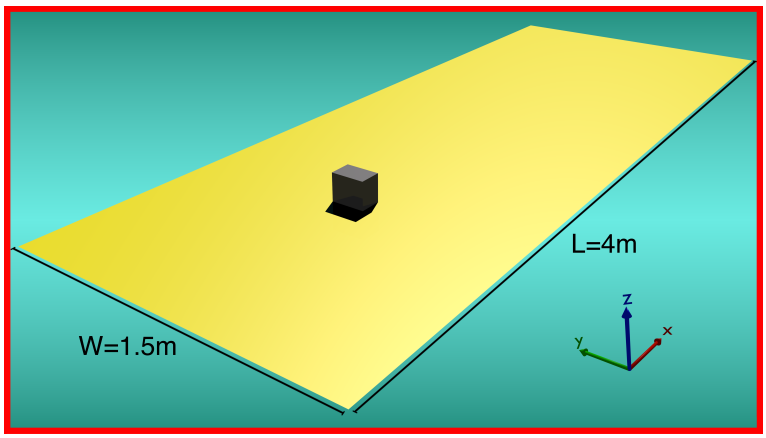

(a)

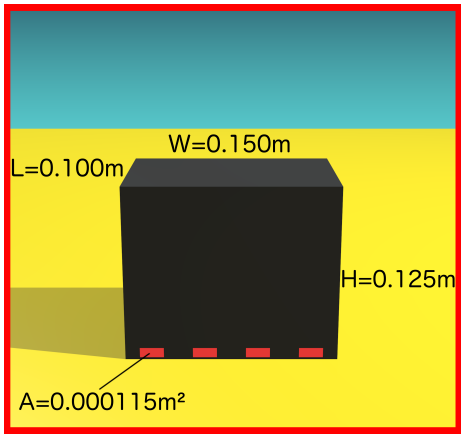

(b)

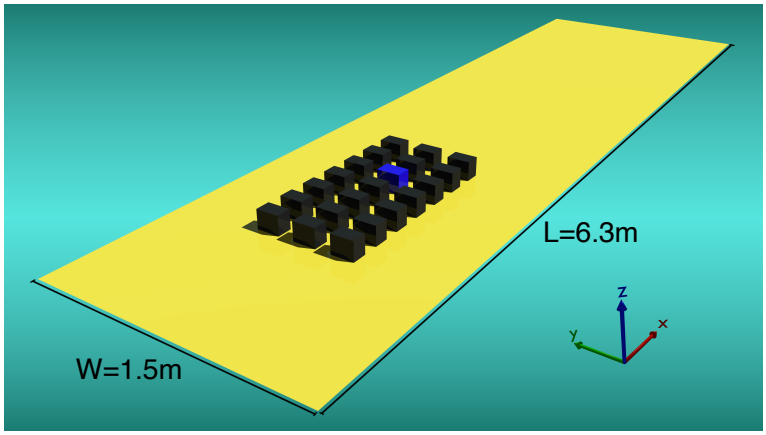

(c)

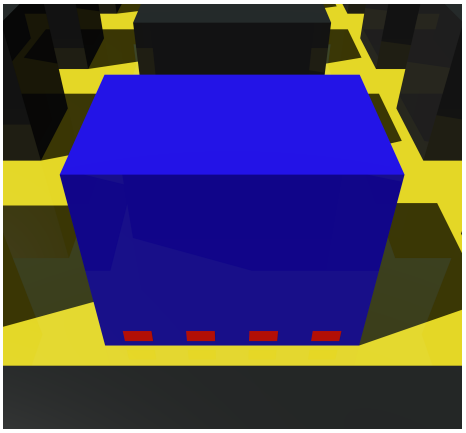

(d)

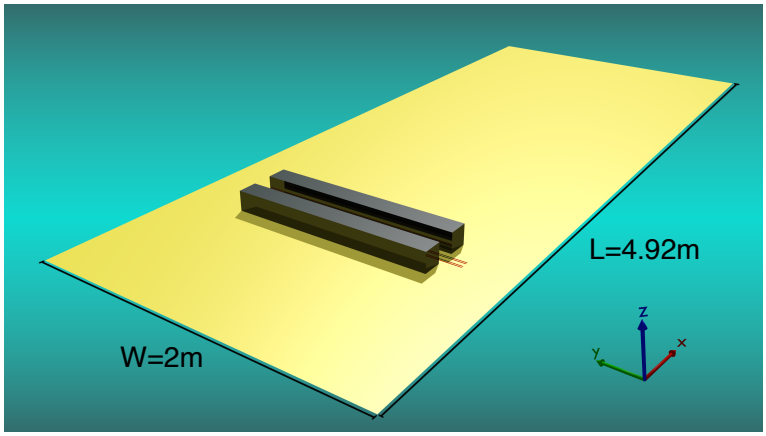

(e)

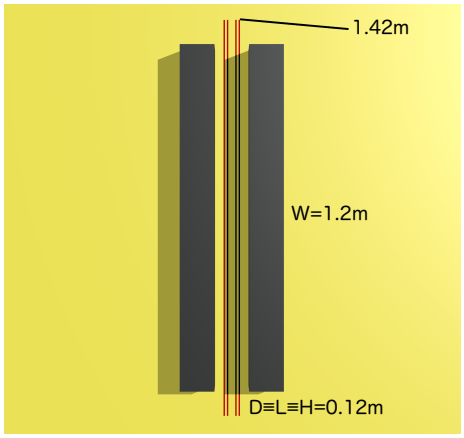

(f)

Figure 1: Cedval A1-5 single building (a-b), B1-1 array of buildings (c-d) and empty street canyon (e-f) test cases. The Cedval single building, the training case for this study, has been marked in red. Subfigures b-d-f display a zoomed view of the source buildings and the pollutant emitting sources (red squares/rectangles). Four sources are located on the leeward side of the emitting buildings for the test cases A1-5/B1-1 (b-d) while four sources are located on the ground, in-between the buildings, for the empty street canyon (f). For all the test cases under study, the pollutant is released simultaneously.

2. Turbulence and dispersion modelling

The CFD investigation of the atmospheric boundary layer is typically carried out by either solving the RANS equations either performing Large-Eddy Simulations (LES). Although LES simulations can lead to better results, they are at least one order of magnitude more expensive than RANS [38, 39]. A compromise between the two approaches is represented by Detached-Eddy Simulations (DES), where unsteady RANS models are employed in the boundary layer, switching to LES treatment in the separated regions.

In the present work, DES is employed to obtain high fidelity data, to retrieve a novel formulation of the Sc_t. Subsequently, the resulting Sc_t is employed and assessed coupled to a modified $k-\epsilon$ closure, designed for ABL flows [40, 41, 39, 42]. It employs a set of boundary conditions and turbulence variables, as expressed in Table 1. The modelling approach is completed by a wall formulation based on the local aerodynamic

Table 1: *Set of inlet conditions and turbulence variables for the "comprehensive approach" [39].*

Inlet Conditions	**Turbulence Model**
$U = \frac{u_*}{\kappa} ln\left(\frac{z+z_0}{z_0}\right)$	$\mu_t = C_\mu \rho \frac{k^2}{\epsilon}$
$k\left(z\right) = C_{k1} ln\left(z+z_0\right) + C_{k2}$	$S_\epsilon\left(z\right) = \frac{\rho u_*^4}{(z+z_0)^2}\left(\frac{(C_{\epsilon 2}-C_{\epsilon 1})\sqrt{C_\mu}}{\kappa^2} - \frac{1}{\sigma_\epsilon}\right)$
$\epsilon\left(z\right) = \frac{u_*^3}{\kappa(z+z_0)}$	$C_\mu = \frac{u_*^4}{k^2}$

roughness [39, 43]. Whenever an obstacle is involved, a Building Influence Area (BIA), i.e. an area where non-linear eddy-viscosity models [44, 45, 46, 47] are applied, is used [40, 39, 43]. The BIA is able to automatically envelope the obstacles immersed in the flow-field.

As for the DES settings, the delayed Detached Eddy Simulation (dDES), proposed by Spalart et al. [48], was employed. With respect to the standard DES, dDES uses a modified lenght scale to remedy the problems of grid-induced separation (GIS) and modelled stress depletion (MSD) [49]. The dDES model chosen for this study is based on the realizable $k-\epsilon$ model. This permitted to use the same boundary conditions imposed for the RANS simulation. In this model the dissipation term is modified as follows:

$$Y_k = \frac{\rho k^{\frac{3}{2}}}{l_{des}}, \tag{1}$$

with:

$$l_{des} = min(l_{rke}, l_{les}), \tag{2}$$

$$l_{rke} = \frac{k^{\frac{3}{2}}}{\epsilon}, \tag{3}$$

$$l_{les} = C_{\mathrm{des}}\Delta, \tag{4}$$

where C_{des} is a calibration constant used in the DES model with a value of 0.61. Δ is the maximum local grid spacing: $\Delta \equiv (\ \Delta x,\ \Delta y,\ \Delta z\ )$. In the event that $l_{des} = l_{rke}$, the expression for the dissipation of the k formulation for the Realizable $k-\epsilon$ model is restored:

$$Y_k = \rho\epsilon. \tag{5}$$

In the delayed DES approach, the DES length l_{des} can be finally redefined according to:

$$l_{des} = l_{rke} - f_d \max(0, l_{rke} - C_{\mathrm{des}}\Delta). \tag{6}$$

As for the concentration field, the dispersion of a pollutant is calculated solving a scalar transport equation for the solute concentration, C [50]. Referring to the Standard Gradient Diffusion Hypothesis (SGDH), the concentration transport equation is reduced to the following conservation equation for RANS approaches:

$$\frac{\partial \bar{C}}{\partial t} + \frac{\partial}{\partial X}\left(\bar{U}\bar{C} - (D_m + D_t)\frac{\partial \bar{C}}{\partial X}\right) = \bar{\dot{C}}_0, \tag{7}$$

or for LES approaches:

$$\frac{\partial \widetilde{C}}{\partial t} + \frac{\partial}{\partial X}\left(\widetilde{U}\widetilde{C} - (D_m + D_t)\frac{\partial \widetilde{C}}{\partial X}\right) = \widetilde{\dot{C}}_0, \tag{8}$$

where dashes and swung dashes express mean and filtered quantities, with $D_m = \nu/Sc$ the molecular diffusion coefficient and $D_t = \nu_t/Sc_t$ the turbulent diffusion coefficient.

Significant uncertainty is associated to the specification of Sc_t [26, 15, 51, 25]. Reynolds [23] proposed a variable formulation based on the molecular Schmidt number and the eddy viscosity ratio:

$$Sc_t = C_1 \exp\left[-C_2 Sc^m \left(\frac{\nu_t}{\nu}\right)^n\right], \tag{9}$$

with C_1, C_2, m and n empirically defined constants.

Gorlé et al. [51] demonstrated that better results are achieved when adopting a variable Sc_t formulation, based on the solution obtained for the flow-field. Previous work by Longo et al. [15] supported this per-

spective and proposed the following local definition for Sc_t:

$$Sc_t = \frac{2C_\mu}{C_0 C^2}, \tag{10}$$

with $C_0 = 2$ and $C = 0.35$, two model parameters optimized through uncertainty quantification (UQ).

Dispersion processes are complex phenomena usually studied through simplified configurations [52]: the isolated building, the street canyon and the array of buildings.

In the present study, three test cases provided with experimental data were considered. The Cedval A1-5 single building [36], the training case, on which the data-driven derivation of a novel Sc_t formulation was carried out, employing a dDES. Subsequently, the Sc_t model was verified in the RANS framework on the same Cedval A1-5 and on two supplementary test cases: the Cedval B1-1 cluster of building [36] and the empty street canyon from the CODASC database [37] (Figure 2).

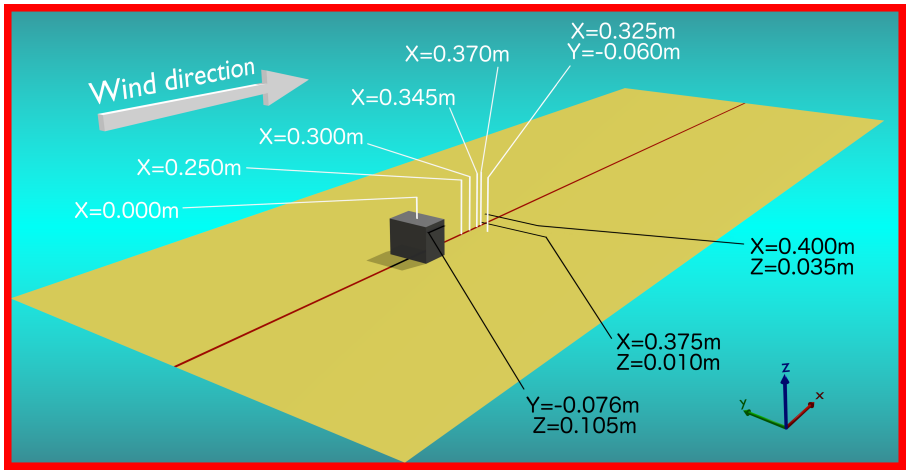

(a)

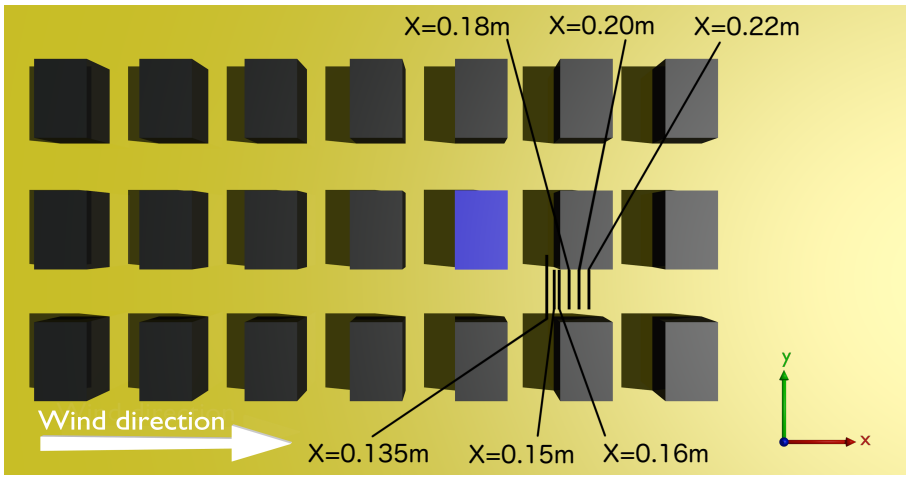

(b)

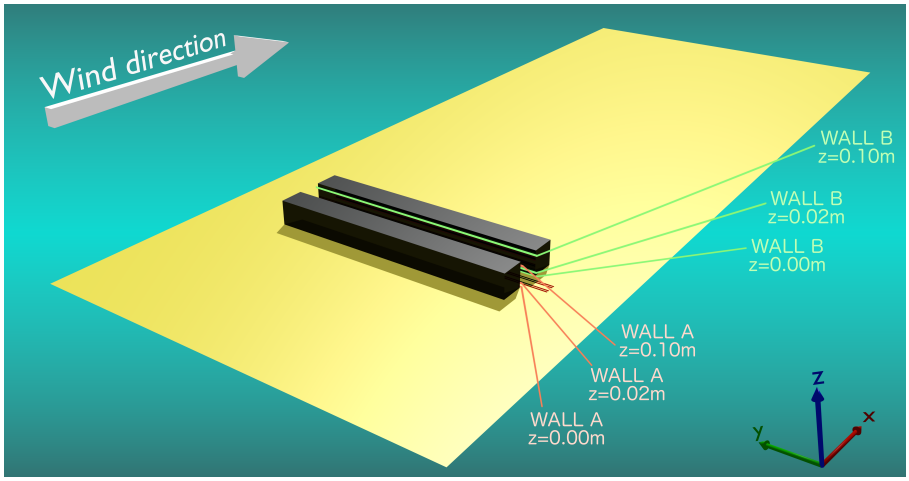

(c)

Figure 2: Test cases under study, including the profile lines taken into consideration for concentration measurements: (a) Cedval A1-5 [39], marked as the training case with a red square

. (b) Cedval B1-1. (c) CODASC empty street canyon.

A brief description of the cases under study follows:

Cedval A1-5 single building - The Cedval A1-5 is the training case, selected for the data-driven derivation, based on the outcomes of a dDES. It features a scaled $1:200$ rectangular single building (Figure 2 (a)). As shown in Figure 1 (b), the building's dimensions are: $L = 0.1m$, $W = 0.15m$ and $H = 0.125m$. The pollutant is emitted simultaneously from 4 source elements located on the leeward facade of the buildings, with a fixed velocity of $U = 0.024$ [m/s]. The roughness length and friction velocity were specified equal to $0.0007m$ and $0.3777m/s$, respectively. Dimensions and precise locations of the source terms are specified in the supplementary material. The origin of the coordinate system is at the center of the bottom face of the building. The z-axis points upwards while the x-axis points downstream. The domain inlet is set $1m$ upstream of the centroid of the building while the outlet is located $3m$ downstream of the origin of the coordinate system [53, 54]. The resulting width and height of the domain are $1.5m$ and $1m$ respectively.

Two different meshes were constructed for the dDES and the RANS simulations. For the dDES approach, the full domain was discretised with a structured mesh consisting of nearly 7 million cells. The grid is refined close to the ground, around the building and the emitting sources. For the grid sensitivity analysis, two additional grids (one coarser and one finer) were built ($r_h = 1.26$). The coarse one resulted in 3.5 million cells and the fine one in 14 million cells. The relative errors of U and k considering the Coarse-Medium and the Medium-Fine meshes were computed to assess the non-dependence of the result from the grid refinement (Table 2).

Table 2: Percentage error of U and k for the three differently refined grids.

Refinement	**Cells [Millions]**	**TKE $\%$ Error**	**U $\%$ Error**
Coarse Mesh (f_3)	3.5	1.65$\%$	1.6$\%$
Medium Mesh (f_2)	7	1.45$\%$	1.45$\%$
Fine Mesh (f_1)	14	–	–

In addition, the GCI between refinement levels and convergence indexes for the two variables was computed:

$$GCI = \frac{F_s \, |e|}{r^{p_c} - 1} \tag{11}$$

where e si the relative error and $p_c = 2$ is the order of convergence. A safety factor $F_s = 1.25$ was assumed [55, 56]. The resulting GCIs are: $\text{GCI}_{12,TKE} = 3.5\%$, $\text{GCI}_{12,U} = 3.4\%$, $\text{GCI}_{23,TKE} = 3\%$, and $\text{GCI}_{23,U} = 3\%$. As for the RANS approach, due to the symmetry of the model with respect to the plane $y = 0m$, only half of the domain was simulated. A structured mesh consisting of approximately 2.4 million cells was adopted. A grid independence study for the same mesh was carried out by Parente et al. [40].

Consequently, mesh, numerical model and settings were considered reliable.

Tunnel sides, ground-mounted building, and tunnel top were set as smooth walls, while the tunnel ground was treated as rough wall. The domain inlet was specified as a velocity inlet, setting the turbulence profiles as specified in Table 1. The end of the domain was defined as pressure outlet.

For the dDES simulation, the synthetic turbulence generator was selected for the fluctuating velocity algorithm. The time step size was set to $6e-5s$, ensuring a CFL number below 0.5, with 22 max iterations per each time step. The simulation was run for the time required for the flow to pass through the domain thrice.

Cedval B1-1 Array of Building - As equally done in previous studies [57], an array of obstacles is analyzed to validate the proposed Sc_t formulations. As shown in Figure 2 (b), it displays a cluster of 3x7 obstacles, with the same dimensions of the A1-5 building. The origin of the Cartesian coordinate system was set at the center of the bottom face of the blue building.

The computational domain extends for $6.3m$, $1.5m$ and $1m$ in the x, y and z directions respectively with the same orientation adopted for the A1-5 test case. The inlet boundary was set $1m$ upstream the first array of buildings, whereas the outlet was located $4m$ downstream of the last array of buildings. The structured mesh consists of 3.8 million cells. A grid sensitivity analysis was carried out in Longo et al. [39]. The boundary conditions were set analogously to the A1-5 test case.

CODASC Empty street canyon - The street canyon from the CODASC dataset [37] involves an empty urban canyon, perpendicular to the inlet velocity, as shown in Figiure 2 (c). Its dimensions are specified in Figure 1 (f), with the distance D between the two internal facades (wall A upwind and wall B downwind) equal to the length L and to the height H of the building, $D = L = H = 0.12m$. The origin of the coordinate system is set at the center of the street canyon. The long side of the building measures $L = 1.2m$. The pollutant is emitted simultaneously from 4 line sources, where each of them is $1.42m$ long. The dimensions of the computational domain are $4.92m$, $2m$ and $1m$ in the x, y and z directions. The inlet is set $8H$ upstream of the first building and the outlet is located $30H$ downstream of the downwind building. The four source lines were modelled as mass-flow inlet, with $Q_s = 0.02kg/s$. z_0 and u_* were specified equal to $0.0033m$ and $0.535m/s$ respectively. The remaining boundary conditions were set analogously to the previous test cases. A structured mesh consisting of 3.5 million hexa cells was built. For the grid sensitivity analysis, one additional grid was built, resulting in 2 million cells (coarsening ratio $r_h = 1.2$). The relative errors for velocity and turbulent kinetic were estimated equal to 0.35% and 0.45% respectively. Whenever comparing two meshes instead of three, a higher safety factor ($F_S = 3$) is advised [55, 56]. A GCI of 2% was determined for velocity and of 3% for turbulent kinetic energy, with respect to the finest grid.

The simulations were performed in ANSYS Fluent 2019 R3. Second-order schemes were set for the momentum, turbulence quantities and the solute concentration, with a coupled scheme for pressure and velocity. Two tracer gases were selected: sulfur dioxide SO_2 for the Cedval test cases A1-5 (single building) and B1-1 (array of building), and sulfur hexafluoride SF_6 for the CODASC urban canyon [58].

3. Manifold-Generated Principal component analysis

The objective of PCA is to extract a smaller set of correlated variables, the principal components (PC), that contain most of the variance of the system. These PCs are a linear combination of the original variables and maximize the information contained in the original state-space [32, 59, 60]. Alternatively, Manifold-Generated PCA is a technique that aims at retaining a subset of original variables instead of transforming the entire state-space to a set of principal components. The smaller set of principal variables (PVs) correlates to the detailed model through the usual PCA matrices. The difference lies in working with a reduced set of the original variables rather than a new set of variables, the principal components.

The technique starts with the extraction of high-fidelity data over the entire computational domain and organizing them in a matrix $\mathbf{X}$. The size of $\mathbf{X}$ equals the number of samples or observations n times the number of conserved variables Q. In this case, the conserved variables are a selection of relevant turbulence parameters such as vorticity and strain rate. These parameters will be detailed in the data extraction and analysis part conducted in Section 4.

MG-PCA solves an eigenvalue problem on the covariance matrix of $\mathbf{X}$ to obtain the eigenvalues, $\mathbf{L}$, and the eigenvectors, $\mathbf{A}$:

$$\mathbf{S} = \mathbf{A}\mathbf{L}\mathbf{A}^{\mathrm{T}}. \tag{12}$$

This matrix of eigenvectors can be truncated to a matrix $\mathbf{A}_q$ containing only a reduced number $q < Q$ of eigenvectors associated with the highest variance in the system. When projecting the original data on this truncated matrix, the principal components are obtained. These correspond to the most influencing variables of the system (Eq. 13). A reconstruction of the original data can be retrieved by inverting the aforementioned relation:

$$\mathbf{Z}_q = \mathbf{X}\mathbf{A}_q, \tag{13}$$

$$\tilde{\mathbf{X}}_q = \mathbf{Z}_q\mathbf{A}_q^{\mathrm{T}}. \tag{14}$$

Manifold-Generated PCA was developed to reconstruct $(Q-q)$ variables of interest from q observed ones. The non-principal reconstructed variables are given by the vector $\tilde{\mathbf{X}}(Q-q)$:

$$\tilde{\mathbf{X}}(Q-q) = \mathbf{X}(q)\mathbf{B}\mathbf{A}(Q-q)_q^{\mathrm{T}}, \tag{15}$$

where $\mathbf{B} = (\mathbf{A}_q^T)^{-1} = \mathbf{X}_q^+ \mathbf{Z}_q$. $\mathbf{X}_q^+$ is the generalized inverse of $\mathbf{X}$, with $\mathbf{X}_q^+ = (\mathbf{X}_q^T \mathbf{X}_q)^{-1}$.
The present paper explores the use of MG-PCA to find a novel formulation for Sc_t as a function of a number of imposed principal variables in the dispersion problem. Consequently, the number of principal variables q equals the number of highly correlated turbulence parameters. In the present case, the variable of interest is Sc_t, meaning that the total number of variables equals $Q = q + 1$, where q will be determined using a correlation study as described later in Section 4. Consequently, Eq. 15 can be rewritten as follows: the reconstructed original variable $\tilde{\mathbf{X}}(Q-q)$ is Sc_t, and the principal variables $\mathbf{X}(q)$ are the subset of correlated turbulent parameters. The matrices $\mathbf{B}\mathbf{A}(Q-q)_q^{\mathrm{T}}$ are specified according to the MG-PCA method.

4. Results

The main objective is to use a data-driven approach in a multi-fidelity framework to derive a local formulation for Sc_t based on a set of general turbulence variables. High-fidelity data are obtained through a dDES on the A1-5 single building case [15] with an optimized local formulation of Sc_t (Eq. 10). Features and correlations are extracted between Sc_t and the turbulence variables. A first model is derived by calibrating the dDES data to the empirical relation proposed by Reynolds [23]. The outcome of this study leads to a correlation analysis in which a set of highly correlated variables are retrieved. Next, these variables are used with MG-PCA to derive an optimal formulation for Sc_t. The new definition for Sc_t is verified with additional CFD simulations on different test cases (Figure 1) employing different turbulence models.
The concentration measurements, used for the model validation, are expressed in dimensionless form. For the Cedval test cases:

$$K = \frac{\left(\frac{C_m}{C_s} U_{ref} H^2\right)}{Q_s} \tag{16}$$

and for the CODASC dataset:

$$K = \frac{(x_i U_{ref} H)}{Q_l} \tag{17}$$

with C_m and C_s the measured and source tracer concentration in ppm; U_{ref}, the reference wind speed in m/s; H, the building height ($0.125m$ fort the Cedval cases and $0.12m$ for the CODASC one); Q_s, total source strength/source flow rate in m^3/s; x_i, the measured tracer molar fraction; and $Q_l \equiv Q_s/L$, the emission rate of line source m^2/s;

4.1. Data from high-fidelity dDES

Data are retrieved from a dDES, employing the ABL inlet conditions. The resulting concentration profiles are displayed in Figure 3. In these profiles, the dDES model coupled with the Sc_t formulation from Eq. 10 is compared to the best-performing RANS approach, namely the ABL turbulence model coupled to the same Sc_t formulation. To verify the effective area of the dDES model where a LES-like approach is applied, it is possible to analyze the dDES TKE dissipation multiplier distribution The latter demonstrates that in the great majority of the domain a high-fidelity approach is retrieved, as reported in the supplementary material.

The overall prediction of the concentration field is improved with the dDES approach. On top of the building (Figure 3 (a-b)) the DES model is able to properly detect the presence of pollutant. In the same location, similar outcomes resulted from a large eddy simulation run by Gorlé et al. [61]. On the contrary, the RANS approach is not detecting any relevant concentration. The almost total lack of pollutant over the building roof was witnessed with all the tested RANS models. This behavior can be attributed to the intrinsic limitations of the RANS modelling approach. In the downwind locations, the under-prediction of concentration is further reduced by the DES method. As the distance from the pollutant sources increases, the behavior of both the DES and RANS becomes comparable.

To analyze the gain in performance resulting from a variable Sc_t in the DES framework and to prove its robustness, Figure 4 shows the concentration from the dDES runs coupled with a constant $Sc_t = 0.4$, the variable Sc_t formulation from Eq. 10, and the LES results by Gorlé et al. [61]. A small under-prediction of the concentration field can be observed for the DES approach with a constant Sc_t. This behavior becomes more accentuated close to the emission location. The comparison demonstrates that the Sc_t plays an equally important role in the DES framework. A similar accuracy was witnessed with respect to the high-fidelity LES results of Gorlé et al. [61].

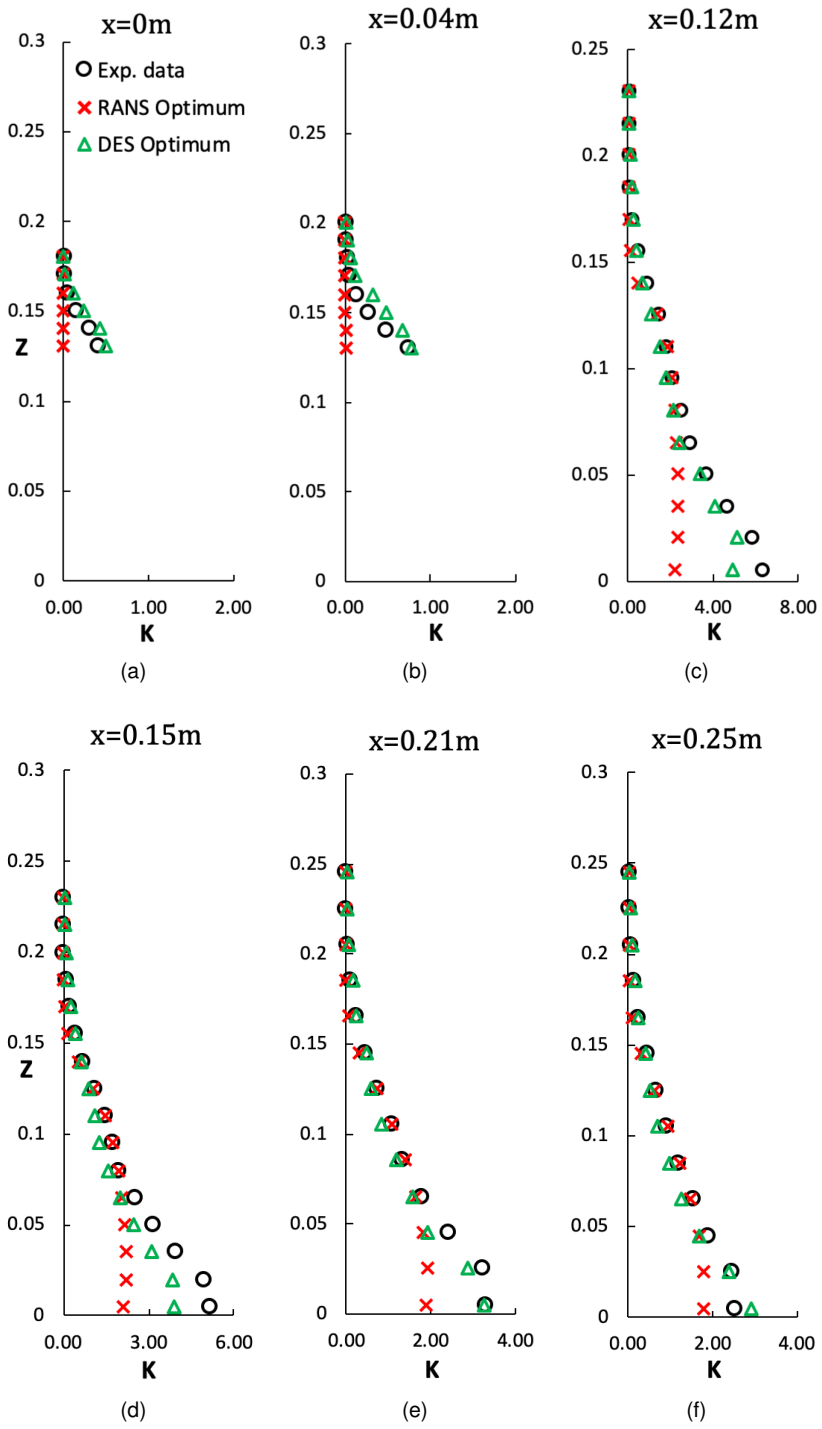

Figure 3: Comparison of experimental and numerical predictions of non-dimensional concentration for the A1-5 test case at different vertical locations in the symmetry plane. The models employed are: the RANS ABL turbulence model coupled to the previously proposed Sc_t formulation 10 (red crosses) and the DES model coupled to the same Sc_t formulation 10 (green triangles).

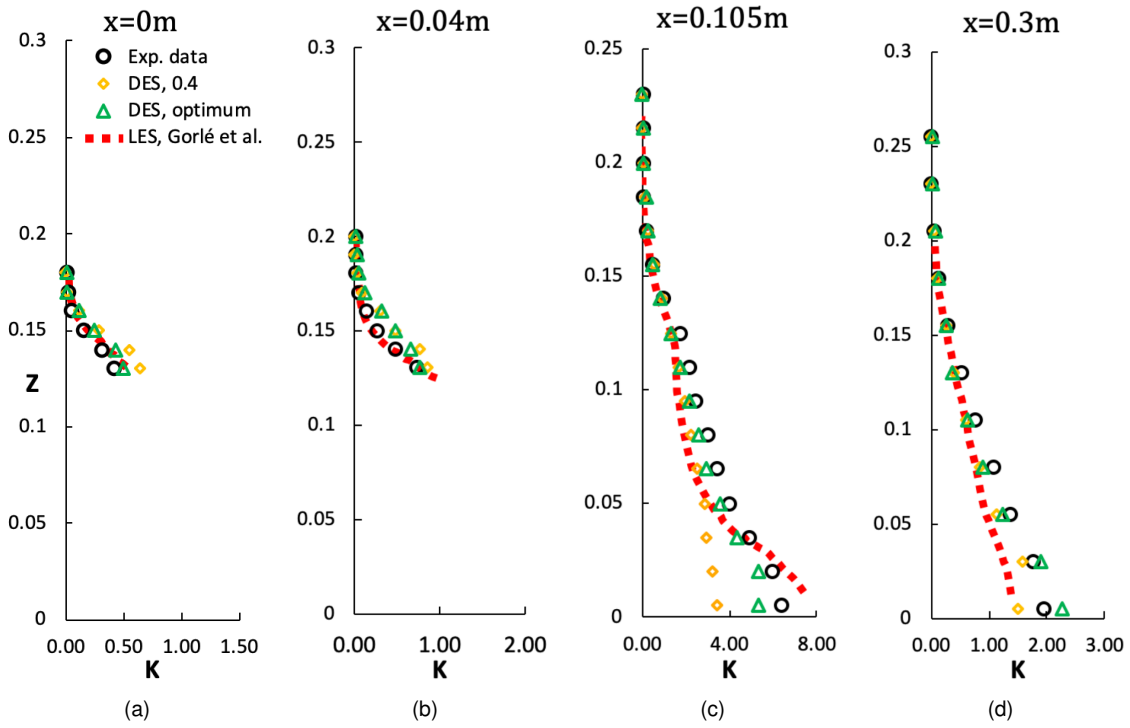

Figure 4: Comparison of experimental and numerical predictions of non-dimensional concentration for the A1-5 test case at different vertical locations in the symmetry plane. The models employed are: the dDES model coupled to the previously proposed Sc_t formulation 10 (green triangles), the dDES model coupled to a constant $Sc_t = 0.4$ (yellow rhombus) and the LES results by Gorlé et al. [61] employing a variable turbulent dispersion coefficient.

4.2. Correlation study and feature-extraction

Reynolds [23] proposed a semi-empirical formulation, tracing the dependency of Sc_t on Sc and the ν_t/ν ratio (Eq. 21). However, there might exist other turbulence variables that show major correlations with Sc_t. The purpose of this investigation is to use the high-fidelity dDES data to verify Reynold's assumption, and to define a larger set of variables showing major dependencies on Sc_t.

To maximize the information contained in the data, the analysis was carried out in planes around the single building of the Cedval A1-5 case. Koeltzsch [24] demonstrated how Sc_t correlates with the height in the boundary layer. Samples were taken at the points corresponding to the experimental locations in the flow field. The test matrix contained ± 1000 observations.

First, the correlation between the Sc_t and a number of flow variables were investigated: the molecular Schmidt number Sc, the Reynolds number Re, the laminar viscosity μ, the turbulent viscosity μ_t, the turbulent kinetic energy k, the turbulent dissipation rate ϵ, the components of the velocity, the laminar Prandtl number, Pr, and the Péclet number, Pe. The objective is to correlate Sc_t with a set of general parameters that are independent of the used turbulence model. Therefore, the turbulent parameter C_μ was not included, as it is a model specific variable.

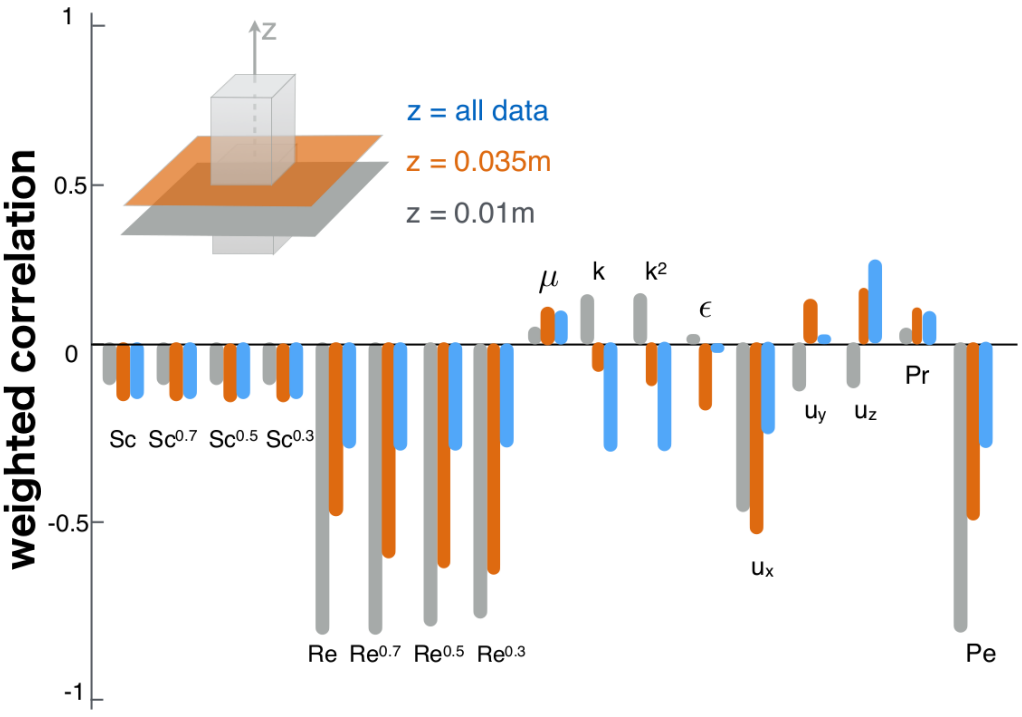

Figure 5: Correlations between Sc_t and the flow variables analyzing the entire domain (blue) and the $z = 0.01$ m (grey) and $z = 0.035$ m (orange) planes.

Figure 5 shows the correlation between Sc_t and the selected flow variables for three different studies: using all the points in the domain, the points in the $z = 0.01m$ plane and the points in the $z = 0.035m$ plane. Sc and Re were raised to the powers 0.7, 0.5 and 0.3. The motivation for raising Sc and Re to an exponent, originates from the empirical formulation of Reynolds where Sc_t is correlated as $Sc_t \approx \exp(Sc^m Re^n)$, with m and n empirically defined constants.

The first conclusion that can be drawn from Figure 5 is that the correlation between Sc_t and other parameters does depend on the boundary layer height. Distinct correlations can be observed in the horizontal planes. However, the variability of the correlations is averaged when studying the entire domain. As a matter of fact, no distinct relation appears between Sc_t and the turbulent variables. This statement changes when focusing on the horizontal planes at the heights $z = 0.01m$ and $z = 0.035m$. Close to the ground, Sc_t correlates with the Reynolds number, the velocity in the x-direction, and the Péclet number,

$$Sc_t \approx \frac{1}{u_x PeRe}. \tag{18}$$

When focusing on the $z = 0.035m$ plane, strong correlation can be observed between Sc_t and the Reynolds number raised to a small exponent and the x-velocity,

$$Sc_t \approx \frac{1}{Re^{0.3} u_x}. \tag{19}$$

Figure 6 compares correlations between Sc_t and various definitions of the Reynolds number: the flow Reynolds number (Re), the Reynolds number at the Taylor scale (Re_λ) and the turbulent Reynolds number (Re_{turb}). Higher correlations are found for the xy-plane close to the ground, $z = 0.01m$. Re_{turb} and Re_λ show similar contributions, and correlate inversely with respect to the flow Reynolds number. Similar behavior is observed for the $z = 0.035m$ plane. When all the points in the data set are considered, all Reynolds numbers correlate in the same direction.

The conclusions drawn from the correlation study are the following: Sc_t shows different correlations with the flow variables depending on the altitude in the boundary layer, according to previous observations [24, 25]. For the 2 horizontal planes in this investigation, major correlations were found with the Reynolds number, the x-velocity and the Péclet number. When all the points are considered in the study, those specific correlations are averaged and no major correlation can be observed.

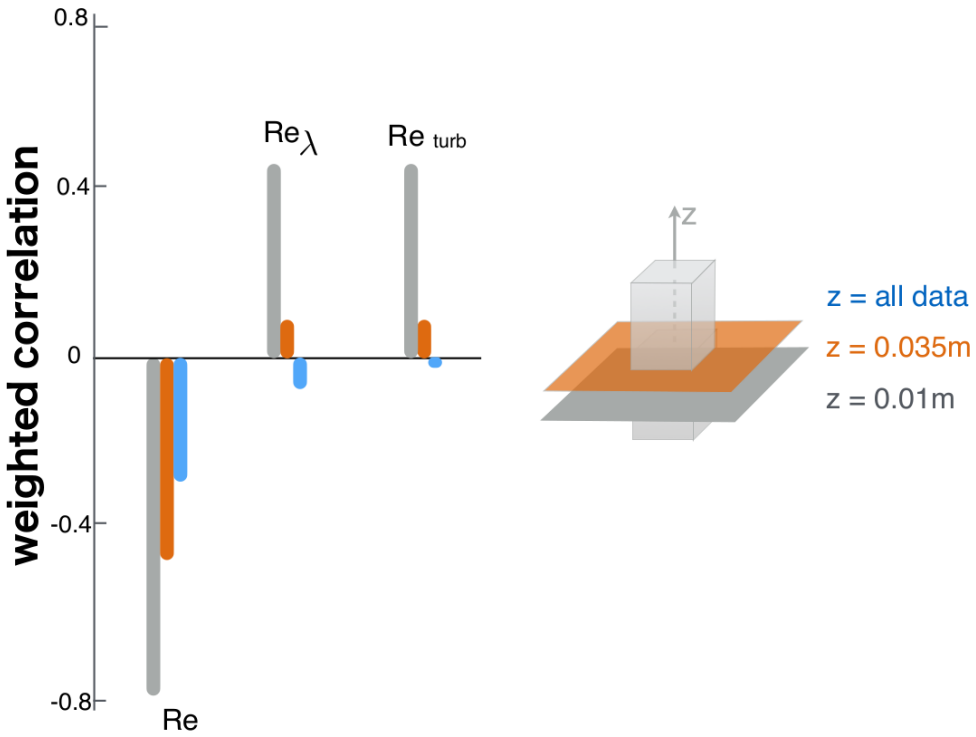

Figure 6: Correlations between Sc_t and the Reynolds number in the entire domain (blue) and in the planes $z = 0.01$ m (grey) and $z = 0.035$ m (orange).

4.3. Model calibration based on empirical relations

A first data-driven formulation for Sc_t was derived through the calibration of the dDES data to an empirical law. Reynolds [23] proposed a formulation to retrieve the turbulent Prandtl number in function of the molecular Prandtl and the turbulent viscosity ratio. This empirical law can be extended to Sc_t as follows,

$$Sc_t = C_1 \exp\left[-C_2 Sc^m \left(\frac{\nu_t}{\nu}\right)^n\right], \tag{20}$$

with (ν_t/ν) the turbulent Reynolds number Re_t, and C_1, C_2, m and n empirically defined constants.

Data for the single building were calibrated to the empirical formulation proposed by Reynolds [23] and verified against the dDES solution with the optimum definition of Sc_t (Eq. 10). Figure 7(a) shows the calibration using the empirical law by Reynolds [23]. Large discrepancies can be observed over the majority of the domain. The large scatter indicates that the combination of the variables proposed by Reynolds [23] does not provide an optimal parametrisation of Sc_t. This further suggests that a more appropriate set of turbulence variables could better correlate with a local formulation of Sc_t.

The local formulation for Sc_t used in the dDES [15] strictly depends on C_μ, a parameter related to the turbulence model employed. Consequently, C_μ could appear as a natural choice to replace the turbulent Reynolds number in the empirical law proposed by Reynolds. However, this parameter strongly depends on the turbulence model formulation. Therefore, a dispersion formulation explicitly requiring C_μ cannot be used in the context of approaches different than the $k-\epsilon$. In this work a calibration to the Reynolds formula is proposed in function of generally available turbulence variables. The Reynolds formula was generalized replacing the turbulent viscosity ratio by the strain invariant S and the vorticity invariant Ω:

$$Sc_t = a \ \exp\left[-b \ \ Sc^c \left(\ d\Omega + \ eS\right)^f\right]. \tag{21}$$

These invariants are included in the C_μ definition employed in the simulation but, differently from this model parameter, they can always be retrieved from the flow field. The coefficients a, b, c, d, e and f are reported in Table 3.

Table 3: Weighting coefficients obtained in a calibration of Sc_t in function of the vorticity and strain invariants (Eq. 21)

a	b	c	d	e	f
2.3361	0.6676	1.130	$1/3$	$2/3$	0.3668

A comparison between the dDES data and the model in Eq. 21 is shown in Figure 7(b). It is clear how the

proposed formulation provides a better parametrisation of Sc_t compared to the original formulation.

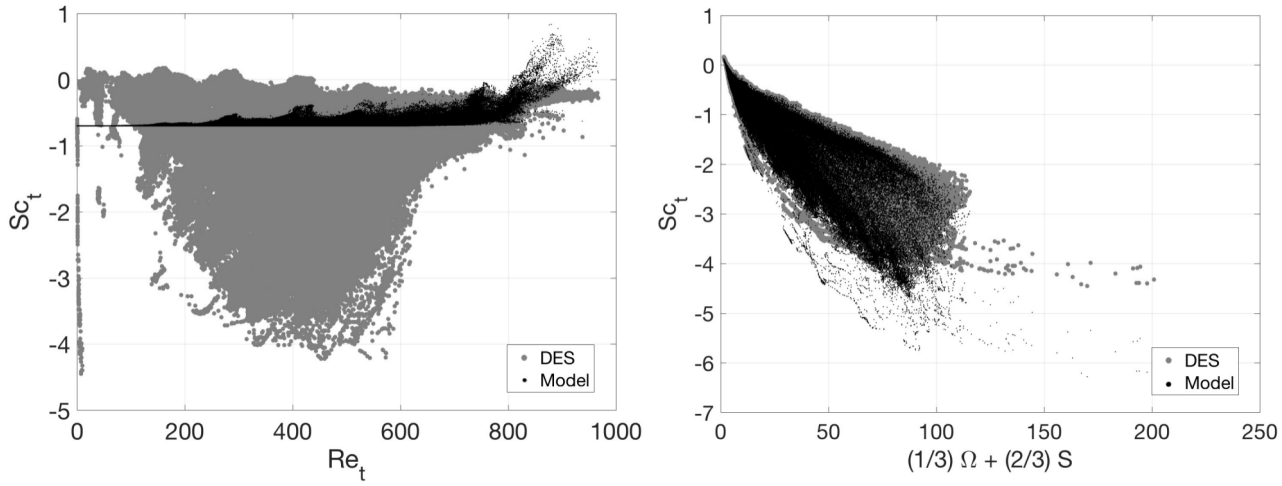

(a) Turbulent Reynolds number

(b) Vorticity and strain rate invariants

Figure 7: Verification of the Reynolds formula against the Cedval A1-5 simulations. The originally imposed correlation with the turbulent Reynolds number (a) is replaced by a linear combination of the strain and vorticity invariants (b).

4.4. Derivation of a generalized Sc_t formulation with MG-PCA

A second data-driven formulation for Sc_t was derived starting from the dDES data. MG-PCA was used to derive a generalized expression of Sc_t based on a number of significant turbulent parameters. These parameters were identified in the correlation study of Section 4.2, and will be imposed as principal variables in the MG-PCA method.

A combination of various flow and turbulence variables were set as principal variables in the MG-PCA according to Eq. 15 with $\tilde{\mathbf{X}}(Q-q) = Sc_t$. In a first instance, the size of matrix $\mathbf{X}$ was $[2,790,457$ x $11]$, as 11 variables were sampled on almost 3 million locations: the molecular Schmidt number, the Reynolds number, the laminar viscosity, the turbulent viscosity, the turbulent kinetic energy, the turbulent dissipation rate, the components of the velocity, the laminar Prandtl number, and the Péclet number. The goal was to retain a relevant selection of variables to obtain the highest correlation with Sc_t. The first step was to consider the variables in the Reynolds formulation, i.e. Re_{turb} and Sc, and, subsequently, add potentially relevant variables one by one in the MG-PCA model while tracking the model R^2 error. The R^2 is an indication for the accuracy of the reconstruction between the simulated Sc_t and the approximation given by the MG-PCA model.

Starting from the empirical formulation by Reynolds [23], the equation was linearised and the logarithm

of the Reynolds formula was taken. This allows to improve the performances of PCA, which is a multi-linear approach, and allows to use the R^2 as an accuracy metric. To verify the Reynolds formula, the error metric was computed for the MG-PCA model using the variables specified in the empirical formula, namely $\log(Sc_t)$, Sc and $Re_{turb}^{0.3}$. A poor correlation of $R^2 = 0.08$ was retrieved. A small improvement was observed by reducing the exponent of the turbulent Reynolds number from 0.3 to 0.01, the resulting R^2 remains unsatisfactory. These results motivate the need for the inclusion of other variables than the ones suggested by Reynolds in the MG-PCA model.

Considering the variables identified in the correlation study, and adding them to the ones identified by Reynolds, it is possible to obtain the following optimized formulation:

$$\log(Sc_t) = a\ Sc - b\ Re_{turb}^{c} - d\ S - e\ \Omega \tag{22}$$

with the a, b, c, d coefficients specified in Table 4.

Table 4: Coefficients for the Sc_t formulation obtained through MG-PCA (Eq. 22), depending on the molecular Schmidt number, on the turbulent Reynolds, on the strain-rate and vorticity invariants

a	b	c	d	e
0.6617	0.8188	0.01	0.0031	0.0329

The final size of matrix $\mathbf{X}$ in the MG-PCA model is therefore [$2,790,457$ x 5]. The constraint of adopting the same turbulence model as the one employed in this study is solved. This is a relevant aspect, considering that this Sc_t formulation can be potentially employed with other turbulence models (LES, DES, RANS: standard-realizable-RNG $k-\epsilon$, $k-\omega$, RSM e.g.), without invalidating its local variability. The latter will be verified in Section 4.5.

4.5. Verification on the selected test cases

The resulting Sc_t formulations trained with the DES data are tested and validated using RANS approaches over the selected test cases: Cedval A1-5 single building, Cedval B1-1 array of buildings and CODASC empty street canyon (Figure 2). They are compared against the constant Sc_t, the formulation proposed by Gorlé et al. [29], and the one by Longo et al. [15]. Additionally, different RANS turbulence closures were tested ranging from the standard ones to the optimised closure for ABL flows.

The main properties of the analyzed pollutants are briefly listed in the supplementary material, while the Sc_t formulations used in this study are presented in Table 5.

Table 5: List of Schmidt formulations and their main parameters employed and compared in this study

Author	**Formulation**	**Parameters**
Standard	$Sc_t = 0.4$	–
Gorlé et al. [29]	$Sc_t = \frac{9}{8} C_\mu C_0$	$C_0 = \frac{C_{0\infty}}{1+7.5 C_{0\infty}^2 Re_\lambda^{-1.64}}$
Longo et al. [15]	$Sc_t = \frac{2C_\mu}{C_0 C^2}$	$C = 0.35$, $C_0 = 2$
Present work (Eq. 21)	$Sc_t = a \left[-b\, Sc^c \left(d\, \Omega + e\, S \right)^f \right]$	a, b, c, d, e, f
Present work (Eq. 22)	$Sc_t = exp\left[a\, Sc + b\, Re_{turb}^c + d\, S + e\, \Omega \right]$	a, b, c, d, e

4.5.1. Cedval A1-5 Single Building

The first set of simulations of the Cedval A1-5 is meant to compare 4 different configurations against the experimental data. This full set of data is plotted in Figure 8:

- standard $k-\epsilon$ model, $Sc_t = 0.4$
- ABL model, Sc_t proposed by Gorlé et al. [29]
- ABL model, Sc_t based on MG-PCA (Eq. 22)
- ABL model, revisited Reynolds [23] Sc_t formulation (Eq. 21).

All the models displaying a variable Sc_t definition show an increased accuracy with respect to a constant Sc_t. As expected, the proposed data-driven Sc_t formulations are able to replicate the performance of the optimal Sc_t (Eq. 10). They show enhanced accuracy with respect to the standard model and a further improvement with respect to the model proposed by Gorlé et al [29].
In Figure 9 (a-c), the standard $k-\epsilon$ model is employed with the Sc_t formulation derived with MG-PCA. Predictably, the variability of the latter is conserved also when an approach displaying a constant C_μ is adopted and permits an increase in the accuracy with respect to the application of a constant Sc_t. Similar observations can be drawn from Figure 9 (d-f), where the MG-PCA approach is applied coupled to the realizable $k-\epsilon$ model and the Reynolds formulation with the Generalized $k-\omega$ model. Both models show similar performance with respect to the optimum approach, namely the one employing the Sc_t proposed by Longo et al. [15]. Additional results for this set of simulations can be found in the supplementary material.

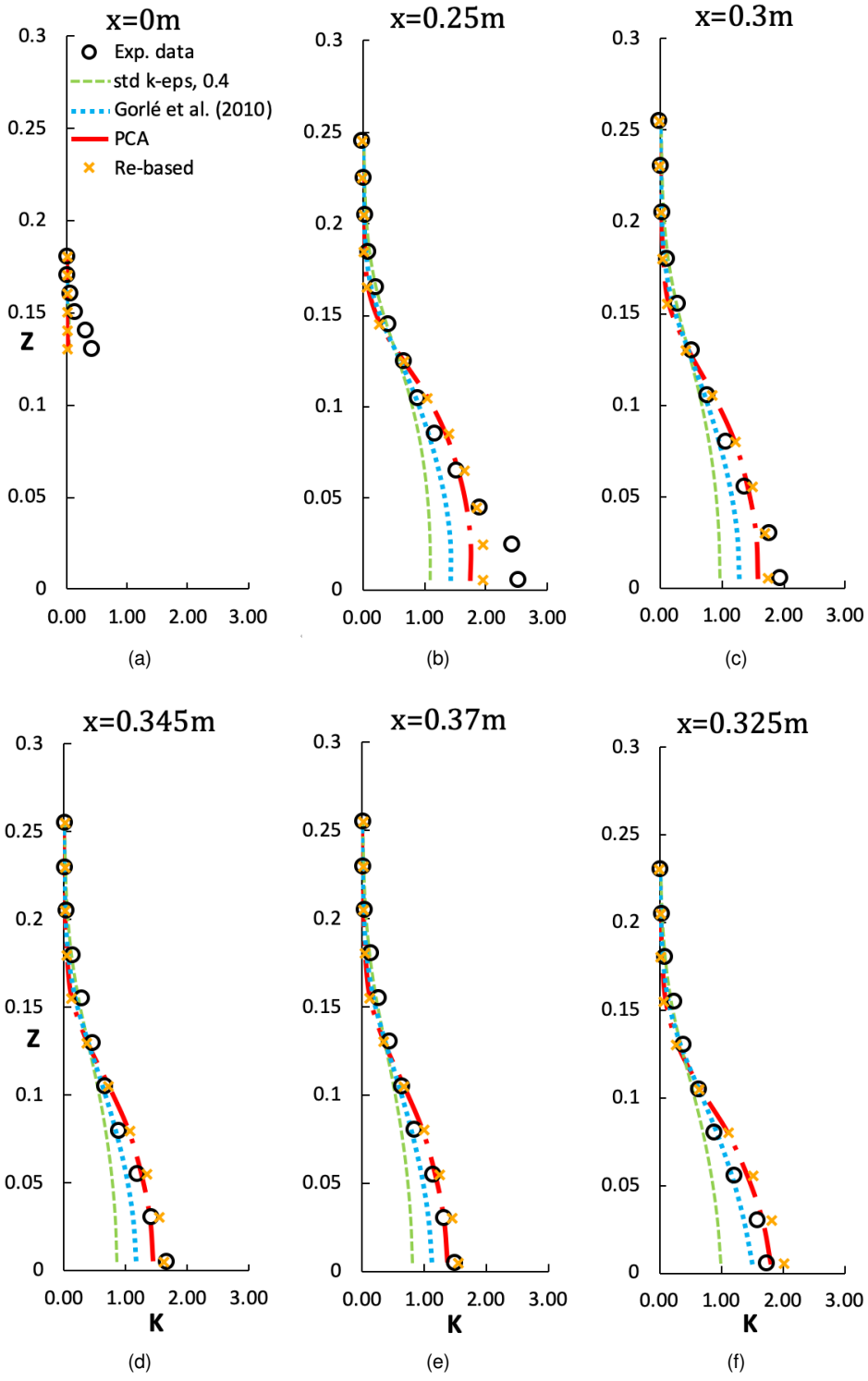

Figure 8: Comparison of experimental and numerical predictions of non-dimensional concentration for the A1-5 test case at different vertical locations, in the symmetry plane (a-e) and in the $y = -0.06m$ plane (f), as displayed in Figure 2 (a). The models used are: the standard $k - \epsilon$ with $Sc_t = 0.4$ (green dashed line), the ABL turbulence model with the Sc_t by Gorlé et al. [29] (light blue dotted line), the ABL turbulence model coupled to the previously proposed Sc_t formulation 10 (red dashed line) and to the one based on Reynolds formulation 21 (orange crosses).

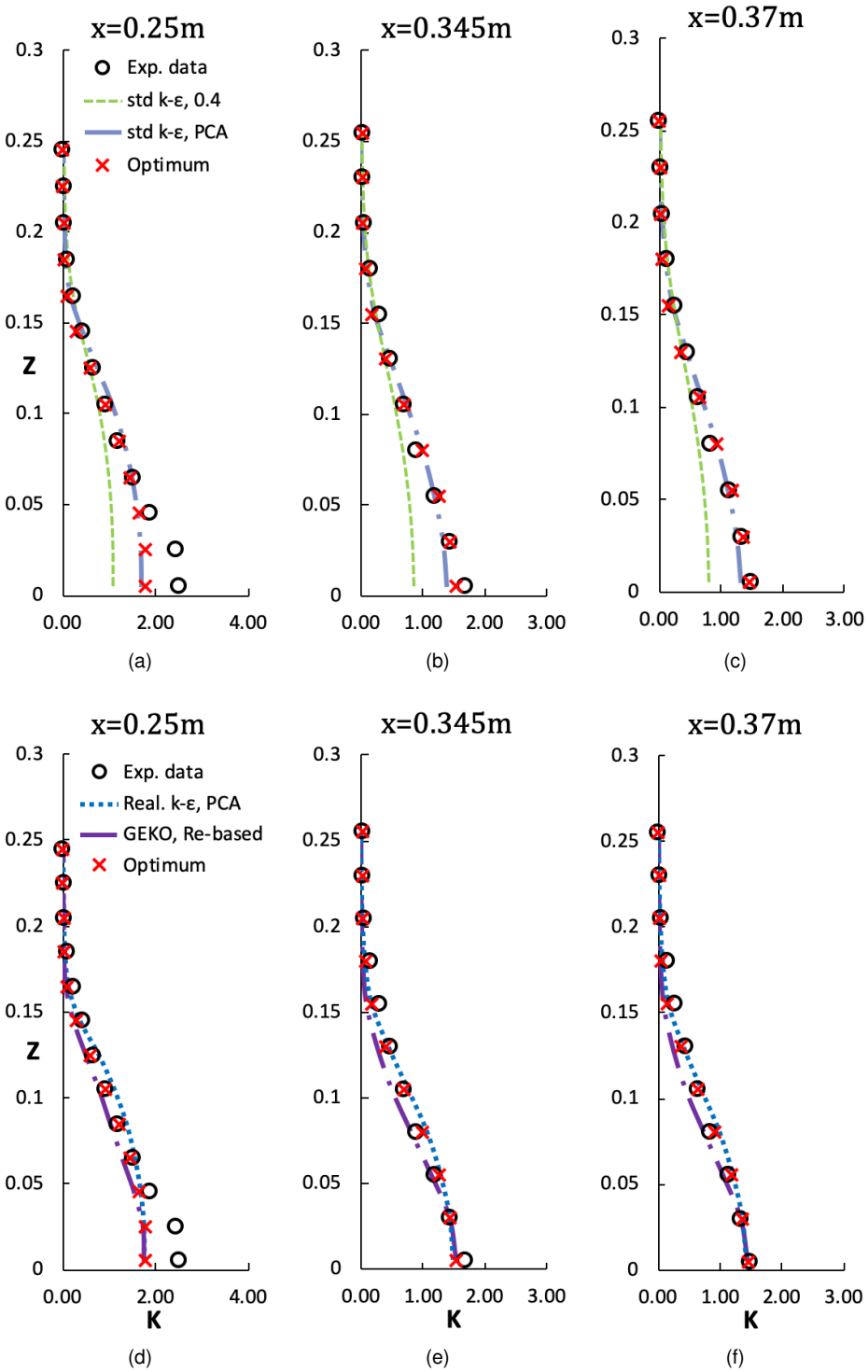

Figure 9: Comparison of experimental and numerical predictions of non-dimensional concentration for the A1-5 test case at different vertical locations, in the symmetry plane, as displayed in Figure 2 (a). On top (a-b-c), the models employed are: the standard $k-\epsilon$ with $Sc_t = 0.4$ (green dashed line), with the MG-PCA formulation (grey broken line), and the ABL turbulence model with the optimum Sc_t formulation 10 (red crosses). On bottom (d-e-f), the models employed include the MG-PCA formulation coupled to the realizable $k-\epsilon$ model (blue dotted line), the Reynolds formulation coupled to GEKO (violet broken line) and the ABL turbulence model coupled to the previously proposed Sc_t formulation 10 (red crosses)

4.5.2. Cedval B1-1 Array of buildings

An array of buildings is considered for validating the proposed methodologies. Experimental profiles are localized, available for the horizontal plane at $7.5mm$ from the ground (Figure 2 (b)).

In Figure 10, the standard $k-\epsilon$ model with $Sc_t = 0.4$ is compared with the ABL turbulence model coupled with the Sc_t by Gorlé et al. [29], the Sc_t resulting from the MG-PCA (Eq. 22) and from the verification of Reynolds formulation (Eq. 21). In the considered locations, the standard $k-\epsilon$ tends to overestimate the concentration field, especially in the downwind locations (Figures 10 (b-f)). When the ABL model is employed, more accurate predictions are witnessed. Specifying Sc_t according to Gorlé et al. [29] leads to a good agreement between predictions and experiments, with respect to the standard methodology.

Good agreement with experimental data is witnessed when using the MG-PCA based Sc_t formulation (red broken line) and from the empirical Reynolds formulation (orange crosses). The over-prediction of the concentration is further limited, resulting in slight discrepancies at few locations (Figure 10 (a)(c)) with an average deviation of 9$\%$ and 6$\%$.

Additional results can be found in the supplementary material.

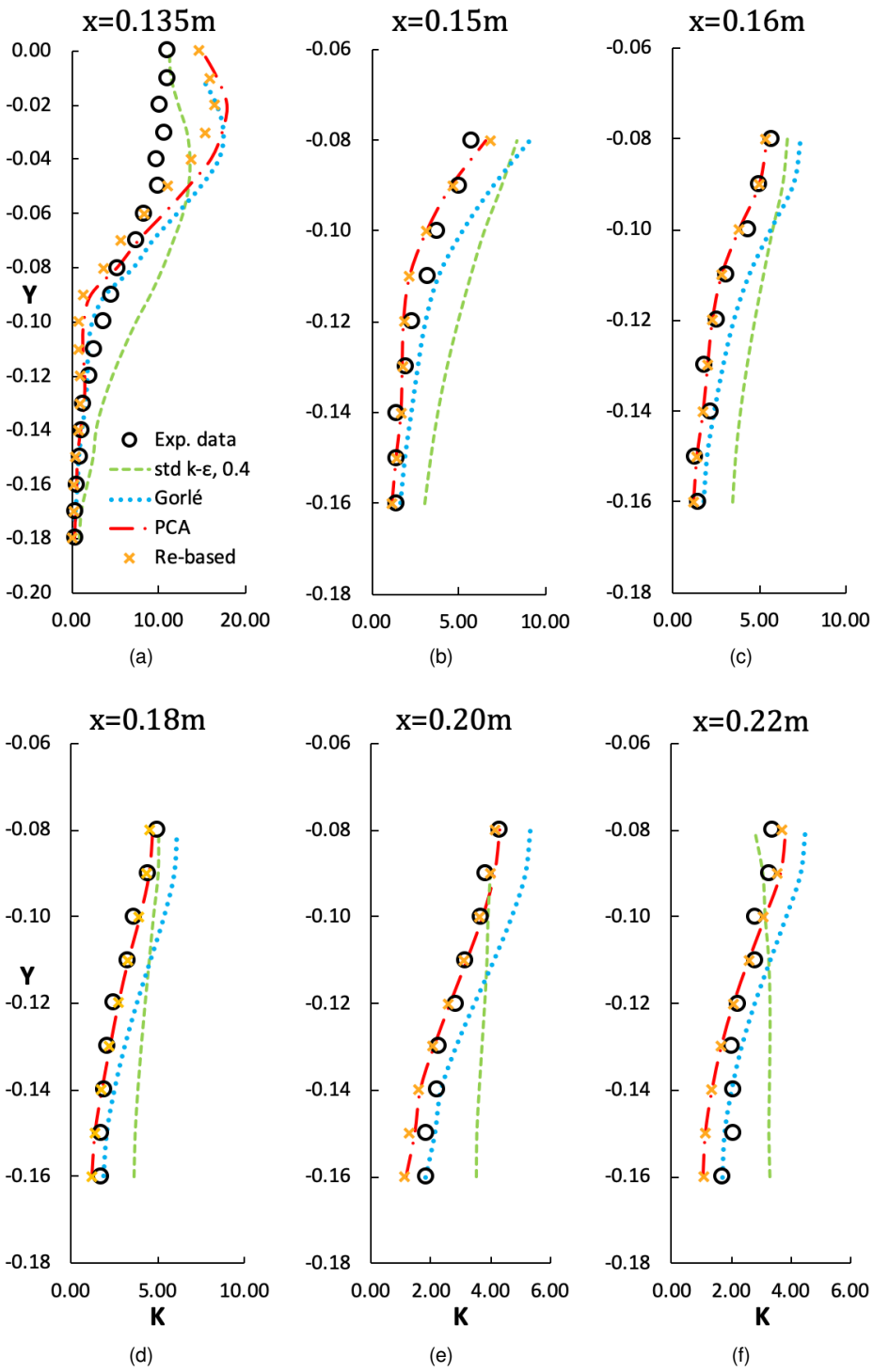

Figure 10: Comparison of experimental and numerical predictions of non-dimensional concentration for the B1-1 test case at different horizontal locations, as displayed in Figure 2 (b). The models used are: the standard $k-\epsilon$ with $Sc_t = 0.4$ (green dashed line), the ABL turbulence model with the Sc_t by Gorlé et al. [29] (light blue dotted line), the ABL turbulence model coupled to the Sc_t formulation based on MG-PCA 22 (red dashed line) and to the one based on Reynolds 21 (orange crosses).

4.5.3. CODASC empty street canyon

Finally, the proposed Sc_t formulations are validated on an empty street canyon case. The performance of the variable formulations are compared to the one of the standard $k-\epsilon$ model with $Sc_t = 0.4$, at three different heights on the internal facades of both the upwind building (building A, measurement plane located at $x = -0.055m$) and the downwind building (building B, measurement plane located at $x = 0.055m$), as shown in Figure 2 (c). The dimensionless concentration profiles are presented in Figure 11. Due to the symmetry of the problem, only half of the profiles ($-0.6m < y < 0m$) are displayed.

It can be observed that the standard methodology tends to overestimate the pollutant concentration. This is especially true close to the ground, where the pollutant is accumulated. One exception to this trend is witnessed at location $z = 0.10m$ on the facade of building B (Figure 11 (f)), where the standard methodology predicts the concentration field accurately. This over-prediction is magnified at the central locations of the wall ($-0.4m < x < 0.4m$).

Even if a certain discrepancy with respect to the experimental data is still observed, more accuracy is shown by the approaches employing the variable Sc_t formulations. Considering the Sc_t proposed in this study, the best agreement with experimental data is witnessed close to the ground. Accurate performance is also shown by the formulation by Gorlé et al. [29]. Once again, the major over-prediction is located at the center of the facades. A similar trend was experienced in previous studies on the same case study [62].

The local variability of the proposed Sc_t based on MG-PCA 22 is demonstrated in the contour plots in Figure 12. Sc_t is ranging according to the local turbulence level, directly depending on Sc, S and Ω.

Additional results can be found in the supplementary material.

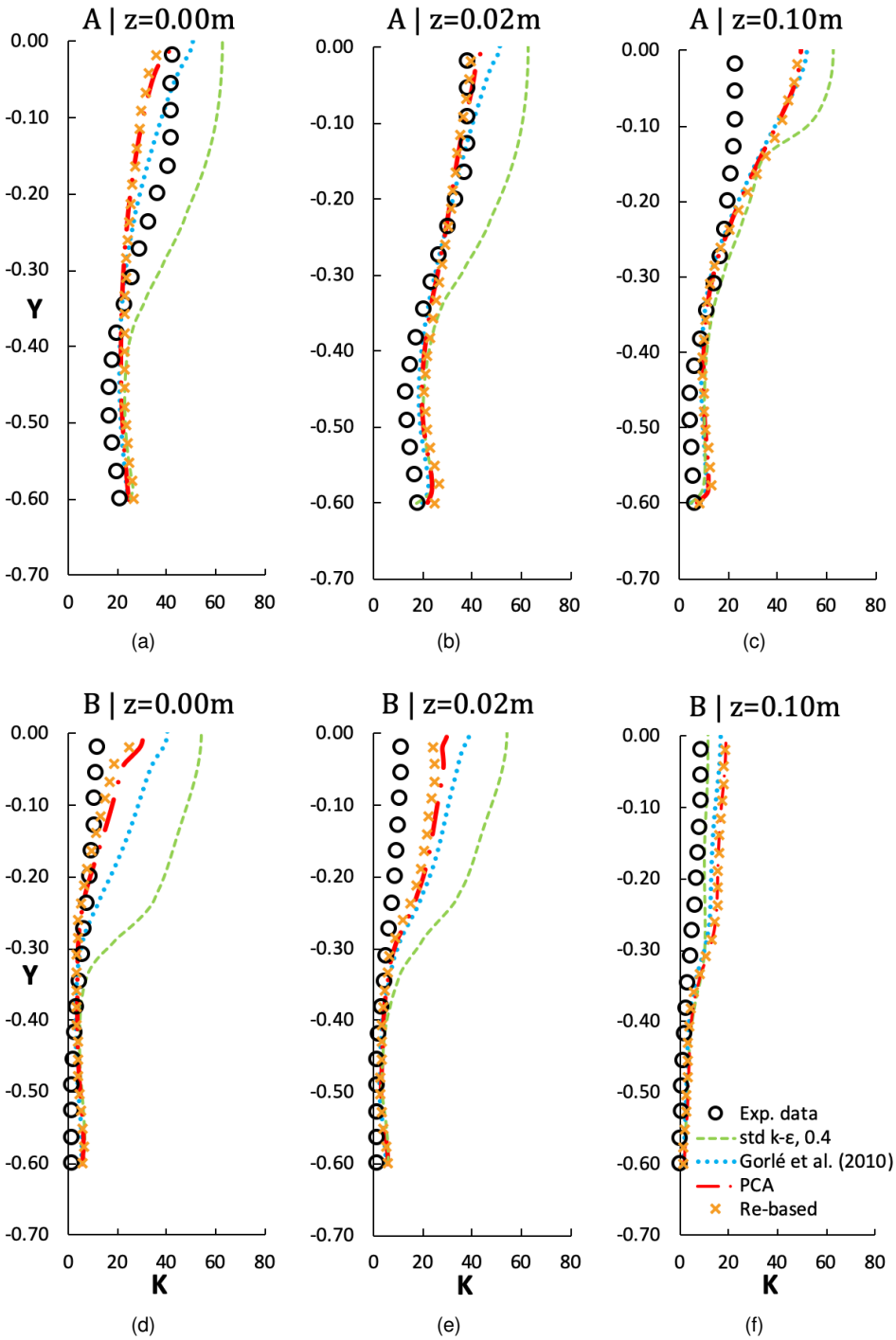

Figure 11: Comparison of experimental and numerical predictions of non-dimensional concentration for the empty street canyon test case at different horizontal axial locations (Figure 2), using the standard $k-\epsilon$ with $Sc_t = 0.4$ (green dashed line), the ABL turbulence model with the MG-PCA Sc_t (red broken line) and the ABL turbulence model coupled to the re-proposed Reynolds formulation depending on vorticity and strain rate (blue dotted line).

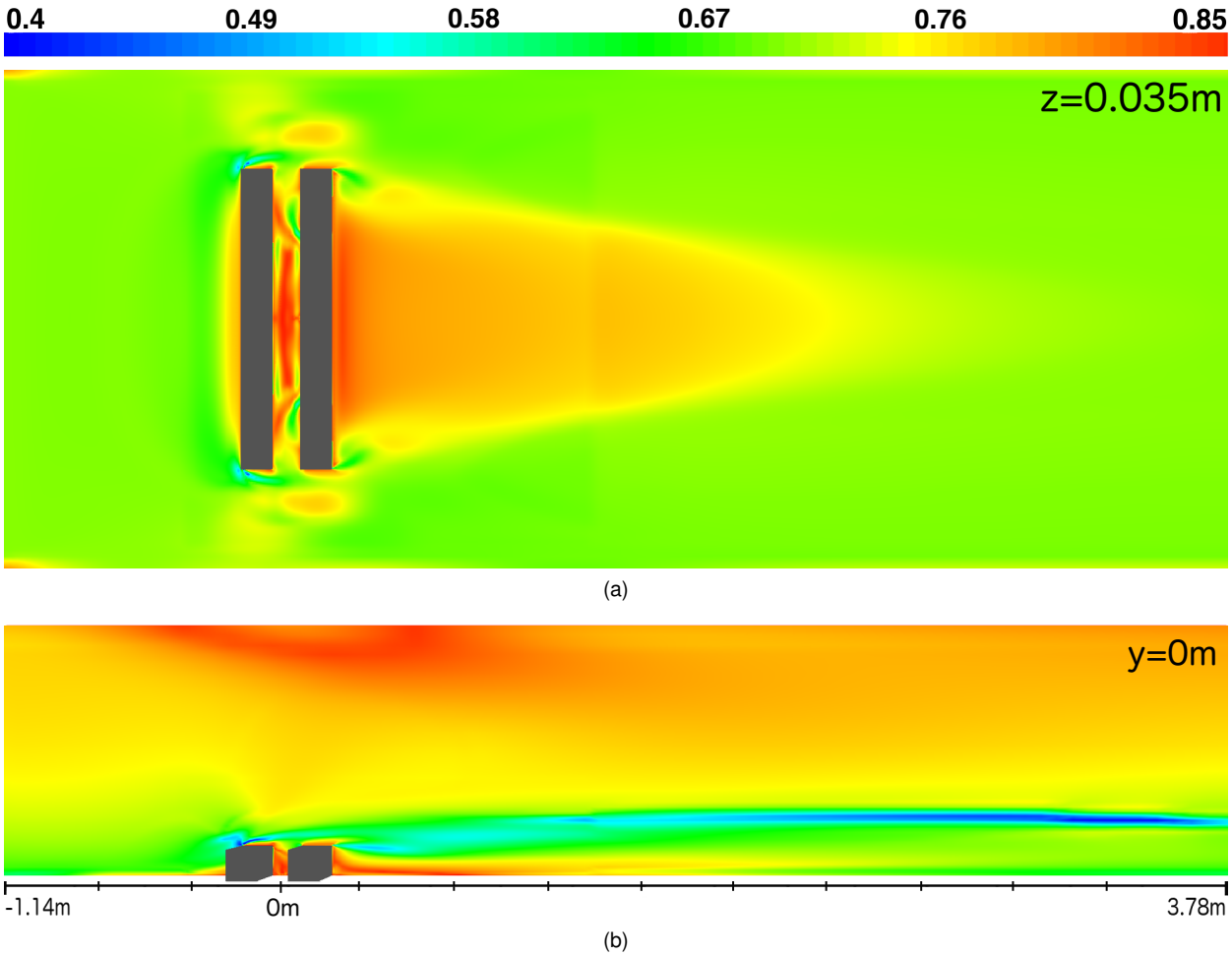

Figure 12: Contour plots of Sc_t derived with MG-PCA (equation 22) for the $90°$ oriented empty street canyon test case from the CODASC dataset in the horizontal $z = 0.035m$ plane (a) and in the vertical $y = 0m$ plane (b). The turbulence approach employed is the ABL RANS model.

5. Conclusion

A comprehensive multi-fidelity framework was presented to derive a local formulation of Sc_t starting from high-fidelity data. dDES were performed on the Cedval A1-5 single building test case to produce a reliable database. These data were used in a correlation study to identify a set of flow and turbulence parameters that identify with Sc_t. A first data-driven model was proposed by calibrating the dDES samples to a semi-empirical formulation proposed by Reynolds. The original formulation by Reynolds was improved by replacing the initial parameters in the model, namely the molecular Schmidt number and the turbulent Reynolds number, by a linear combination of the strain and vorticity invariants. A second formulation was derived by correlating a set of model variables, i.e. the molecular Schmidt number, the turbulent Reynolds number, the strain rate invariant and the vorticity invariant, using Manifold Generated-PCA. In total, 2 new variable turbulent Schmidt formulations were proposed in this study. Both formulations were verified with lower-fidelity RANS simulations on the Cedval A1-5 single building test case, and two additional test cases, namely the Cedval B1-1 array of building, and an empty canyon of the CODASC database. Moreover, the compatibility of the model was verified in combination with various turbulence approaches. The two data-driven models were compared with simulations using a constant Sc_t, and several local formulations proposed previously in the literature. The resulting Sc_t numbers, based on the calibration of the Reynolds-like formula and on Manifold Generated-PCA, capture most of the dependencies observed for the Sc_t in literature, fall in the expected range of atmospheric Sc_t values and are able to improve substantially the prediction of the concentration field. In this regard, the prediction of the concentration field was improved up to 100%, when the variable Schmidt number formulations were applied with both the ABL and standard turbulence models.

Future work will further investigate the use of turbulence models that account for the anisotropic character of the turbulent dispersion. Moreover non-neutral atmospheric stability conditions and more challenging test cases in terms of orography will be analyzed.

[1] F. Karagulian, C. A. Belis, C. F. Dora, A. M. Prüss-Ustün, S. Bonjour, H. Adair-Rohani, and M. Amann. Contributions to cities' ambient particulate matter (pm): A systematic review of local source contributions at global level. *Atmospheric environment*, 120:475–483, 2015.

[2] M. Pontiggia, G. Landucci, V. Busini, M. Derudi, M. Alba, M. Scaioni, S. Bonvicini, V. Cozzani, and R. Rota. Cfd model simulation of lpg dispersion in urban areas. *Atmospheric Environment*, 45:3919–3923, 2011.

[3] M. Pontiggia, M. Derudi, M. Alba, M. Scaioni, and R. Rota. Hazardous gas releases in urban areas: Assessment of consequences through cfd modelling. *Journal of Hazardous Materials*, 176:589–596, 2010.

[4] V. Busini and R. Rota. Influence of the shape of mitigation barriers on heavy gas dispersion. *Journal of Loss Prevention in the Process Industries*, 29:13–21, 2014.

[5] M. Derudi, D. Bovolenta, V. Busini, and R. Rota. Heavy gas dispersion in presence of large obstacles: selection of modeling tools. *Industrial & Engineering Chemistry Research*, 53(22):9303–9310, 2014.

[6] G. Landucci, A. Tugnoli, V. Busini, M. Derudi, R. Rota, and Cozzani V. The viareggio lpg accident: Lessons learnt. *Journal of Loss Prevention in the Process Industries*, 24:466–476, 2011.

[7] V. Busini, M. Pontiggia, M. Derudi, G. Landucci, V. Cozzani, and R. Rota. Safety of lpg rail transportation. *IChemical Engineering Transactions*, 24, 2011.

[8] P. Piroozmand, G. Mussetti, J. Allegrini, M. Haji Mohammadi, E Akrami, and J. Carmeliet. Coupled cfd framework with mesoscale urban climate model: Application to microscale urban flows with weak synoptic forcing. *Journal of Wind Engineering and Industrial Aerodynamics*, 197:–, 2020.

[9] Rota R. and G. Nano. *Introduzione alla Affidabilità e Sicurezza nell'Industria di Processo*. Pitagora Editrice Bologna, 2007.

[10] C. García-Sánchez, D.A. Philips, and C. Gorlé. Quantifying inflow uncertainties for cfd simulations of the flow in downtown oklahoma city. *Building and Environment*, 78:118–129, 2014.

[11] X. Yang and F. Sotiropoulos. On the dispersion of contaminants released far upwind of a cubical building for different turbulent inflows. *Building and Environment*, 154:324–335, 2019.

[12] T. van Hooff, B. Blocken, and Y. Tominaga. On the accuracy of cfd simulations of cross-ventilation flows for a generic isolated building: Comparison of rans, les and experiments. *Building and Environment*, 114:148–165, 2017.

[13] B. Blocken and C. Gualtieri. Ten iterative steps for model development and evaluation applied to computational fluid dynamics for environmental fluid mechanics. *Environmental Modelling & Software*, 33:1–22, 2012.

[14] F. Li, J. Liu, J. Ren, and X. Cao. Predicting contaminant dispersion using modified turbulent schmidt numbers from different vortex structures. *Building and Environment*, 130:120–127, 2018.

[15] R. Longo, M Fürst, A Bellemans, M. Ferrarotti, M. Derudi, and A. Parente. Cfd dispersion study based on a variable schmidt formulation for flows around different configurations of ground-mounted buildings. *Building and Environment*, 2019.

[16] T. K. Flesh, J. H. Prueger, and J. Hatfield. Turbulent schmidt number from a tracer experiment. *Agricultural and Forest Meteorology*, 111:299–307, 2002.

[17] C. Gualtieri and F. A. Bombardelli. Parameterization of the turbulent schmidt number in the numerical simulation of turbulent open channel flows. 2013.

[18] A. Riddle, D. Carruthers, A. Sharpe, C. McHugh, and J. Stocker. Comparisons between fluent and adms for atmospheric dispersion modelling and flow around bluff bodies. *Atmospheric Environment*, 38:1029–1038, 2004.

[19] S. Di Sabatino, R. Buccolieri, B. Pulvirenti, and R. Britter. Simulations of pollutant dispersion within idealised urban-type geometries with cfd and integral models. *Atmospheric environment*, 41(37):8316–8329, 2007.

[20] B. Blocken, T. Stathopoulos, P. Saathoff, and X. Wang. Numerical evaluation of pollutant dispersion in the built environment: comparisons between models and experiments. *Journal of Wind Engineering and Industrial Aerodynamics*, 96(10-11):1817–1831, 2008.

[21] N. Reiminger, J. Vazquez, N. Blond, M. Dufresne, and J. Wertel. Cfd evaluation of mean pollutant concentration variations in step-down street canyons. *Journal of Wind Engineering and Industrial Aerodynamics*, 196:–, 2020.

[22] Y. Tominaga and T. Stathopoulos. Turbulent schmidt numbers for cfd analyis with various types of flowfield. *Atmos. Environ.*, 41:8091–8099, 2007.

[23] A.J. Reynolds. The prediction of turbulent prandtl and schmidt numbers. *Int. J. Heat Mass Transfer*, 18:1055–1069, 1975.

[24] K. Koeltzsch. The height dependence of the turbulent schmidt number within the boundary layer. *Atmospheric Environment*, 34(7):1147–1151, 2000.

[25] A. Di Bernardino, P. Monti, G. Leuzzi, and G. Querzoli. Turbulent schmidt number measurements over three- 3 dimensional cubic arrays. *Boundary-Layer Meteorology*, 2019.

[26] C. Gualtieri, A. Angeloudis, F. Bombardelli, S. Jha, and T. Stoesser. On the values for the turbulent schmidt number in environmental flows. *Fluids*, 2(2):17, 2017.

[27] Z. Shi, J. Chen, and Q. Chen. On the turbulence models and turbulent schmidt number in simulating stratified flows. *Journal of Building Performance Simulation*, 9:134–148, 2016.

[28] C. Trägårdh C. Rosén. Prediction of turbulent high schmidt number mass transfer using a low reynolds number $k - \epsilon$ turbulence model. *The Chemical Engineering Journal*, 59:153–159, 1995.

[29] C. Gorlé, J. van Beeck, and P. Rambaud. Dispersion in the wake of a rectangular building: validation of two reynolds-averaged navier–stokes modelling approaches. *Boundary-layer meteorology*, 137(1):115–133, 2010.

[30] M. G. Fernández-Godino, C. Park, N.-H. Kim, and R. T. Haftka. Review of multi-fidelity models. *arXiv preprint arXiv:1609.07196*, 2016.

[31] C. Huang, W. E. Anderson, C. L. Merkle, and V. Sankaran. Multi-fidelity framework for modeling combustion instability. Technical report, AFRL/RQR Edwards AFB United States, 2016.

[32] A. Parente and J. Sutherland. Prinicpal component analysis of turbulent combustion data: Data pre-processing and manifold sensitivity. *Combustion and Flame*, 160(2):340–350, 2013.

[33] B. Isaac, A. Coussement, O. Gicquel, P. J. Smith, and A. Parente. Reduced-order pca models for chemical reacting flows. *Combustion and Flame*, 161(11):2785 – 2800, 2014.

[34] A. Bellemans, A. Munafo, T.E. Magin, G. Degrez, and A. Parente. Reduction of a collisional-radiative mechanism for argon plasma based on principal component analysis. *Physics of plasmas*, 22(6):062108, 2015.

[35] A. Coussement, B. J. Isaac, O. Gicquel, and A. Parente. Assessment of different chemistry reduction methods based on principal component analysis: Comparison of the mg-pca and score-pca approaches. *Combustion and Flame*, 168:83–97, 2016.

[36] Hamburg University. Cedval at hamburg university compilation of experimental data for validation of microscale dispersion models, website provided by the environmental wind tunnel laboratory (ewtl) of the meteorological institute. `http://www.mi.zmaw.de/index.php?id=628`.

[37] University of Karlsruhe. Codasc stands for "concentration data of street canyons". codasc data is from the laboratory of building- and environmental aerodynamics at the institute for hydromechanics (ifh) at the university of karlsruhe/germany. `https://www.windforschung.de/CODASC.htm`.

[38] W. Rodi. Comparison of les and rans calculations of the flow around bluff bodies. *Journal of wind engineering and industrial*

aerodynamics, 69:55–75, 1997.

[39] R. Longo, M. Ferrarotti, C. García-Sánchez, M. Derudi, and A. Parente. Advanced turbulence models and boundary conditions for flows around different configurations of ground-mounted buildings. *Journal of wind engineering and industrial aerodynamics*, 167:160–182, 2017.

[40] A. Parente, C. Gorlé, J. van Beeck, and C. Benocci. A comprehensive modelling approach for the neutral atmospheric boundary layer: Consistent inflow conditions, wall function and turbulence model. *Boundary-Layer Meteorology*, 140:411, 2011.

[41] A. Parente, R. Longo, and Ferrarroti M. Cfd boundary conditions, turbulence models and dispersion study for flows around obstacles. In *VKI Lecture Series*, 2017.

[42] E. Keshavarzian, R. Jin, K. Dong, K. C. S. Kwok, Y. Zhang, and M. Zhao. Effect of pollutant source location on air pollutant dispersion around a high-rise building. *Applied Mathematical Modelling*, 81:582–602, 2020.

[43] R. Longo, P. Nicastro, M. Natalini, P. Schito, R. Mereu, and A. Parente. Impact of urban environment on savonius wind turbine performance: a numerical perspective. *Renewable Energy*, -:–, 2020.

[44] T. J. Craft, B. E. Launder, and K. Suga. Development and application of a cubic eddy-viscosity model of turbulence. *International Journal of Heat and Fluid Flow*, 17(2):108–115, 1996.

[45] F. S. Lien, W. L. Chen, and M. A. Leschziner. Low-reynolds-number eddy-viscosity modelling based on non-linear stress-strain/vorticity relations. In *Engineering Turbulence Modelling and Experiments, Volume 3*, pages 91–100. Elsevier, 1996.

[46] J. Ehrhard and N. Moussiopoulos. On a new nonlinear turbulence model for simulating flows around building-shaped structures. *Journal of Wind Engineering and Industrial Aerodynamics*, 88(1):91–99, 2000.

[47] W. Bauer, W. Haag, and D.K. Hennecke. Accuracy and robustness of nonlinear eddy viscosity models. *International Journal of Heat and Fluid Flow*, 21:312–319, 2000.

[48] P.R. Spalart, S. Deck, M.L. Shur, K.D. Squires, M.K. Strelets, and A. Travin. A new version of detached-eddy simulation, resistant to ambiguous grid densities. *Theor Comput Fluid Dyn*, 20:181–195, 2006.

[49] J. Gao and X. Li. Implementation of delayed detached eddy simulation method to a high order spectral difference solver. *Computers & Fluids*, 154:90–91, 2017.

[50] P. Ouroi, B. Fraga, N. Viti, A. Angeloudis, T. Stoesser, and C. Gualtieri. Instantaneous transport of a passive scalar in a turbulent separated flow. *Environ Fluid Mech*, 2017.

[51] C. Gorlé, J. van Beeck, P. Rambaud, and G. Van Tendeloo. Cfd modelling of small particle dispersion: the influence of the turbulence kinetic energy in the atmospheric boundary layer. *Atmospheric Environment*, 43(3):673–681, 2009.

[52] B. Blocken, T. Stathopoulos, and J. Carmeliet. Cfd simulation of micro-scale pollutant dispersion in the built environment. *Building and Environment*, 66:225–230, 2013.

[53] Yoshihide Tominaga, Akashi Mochida, Ryuichiro Yoshie, Hiroto Kataoka, Tsuyoshi Nozu, Masaru Yoshikawa, and Taichi Shirasawa. Aij guidelines for practical applications of cfd to pedestrian wind environment around buildings. *Journal of Wind Engineering and Industrial Aerodynamics*, 96:1749–1761, 2008.

[54] J. Franke, C. Hirsch, A. G. Jensen, H. W. Krüs, M. Schatzmann, P. S. Westbury, S. D. Miles, J. A. Wisse, and N. G. Wright. Recommendations on the use of cfd in wind engineering. In *Cost action C*, volume 14, page C1, 2004.

[55] Roache P.J. *Verification and validation in computational science and engineering*. Hermosa Publishers, Albuquerque, NM, USA, 1998.

[56] Patrick J Roache. Perspective: Validation—what does it mean? *Journal of Fluids Engineering*, 131(3):034503, 2009.

[57] Y. Dai, C. M. Mak, Z. Ai, and J. Hang. Evaluation of computational and physical parameters influencing cfd simulations of

pollutant dispersion in building arrays. *Building and Environment*, 137:90–107, 2018.

[58] C. Gromke and B. Ruck. Influence of trees on the dispersion of pollutants in an urban street canyon - experimental investigation of the flow and concentration field. *Atmos. Environ.*, 41:3387–3302, 2007.

[59] S. Park and S. Y. Jung. Principal component analysis of water pipe flow data. *Procedia Engineering*, 89:395–400, 2014.

[60] K. Pandžić and D. Trninić. Principal component analysis of a river basin discharge and precipitation anomaly fields associated with the global circulation. *Journal of Hydrology*, 132:343–360, 1992.

[61] C. Gorlé, P. Rambaud, and J. van Beeck. Large eddy simulation of flow and dispersion in the wake of a rectangular building. 2010.

[62] M. S. Salim, A. Chan, R. Buccolieri, and S. Di Sabatino. *CFD Study on the Roles of Trees on Airflow and Pollutant Dispersion within Urban Street Canyons*. International Energy and Environmental Foundation, 2011.